ARMA 13-305

Modeling Stiffness Anisotropy Induced by Crack Opening in Rocks Subjected to Thermal versus Mechanical Stress Gradients

Zhu, C., Arson, C., and Xu, H.
Geosystems group, School of Civil and Environmental Engineering,
Georgia Institute of Technology, Atlanta, Georgia, USA.

ABSTRACT: A thermodynamic framework is proposed to model the coupled effects of mechanical and thermal stresses in rocks. The model is based on Continuum Damage Mechanics with damage defined as the second-order crack density tensor. The free energy of damaged rock is expressed as a function of deformation, temperature, and damage. The damage criterion controls mode I crack propagation, captures temperature-induced decrease of rock toughness, and accounts for the increase of energy release rate necessary to propagate cracks in a damaged medium. Two loading paths have been simulated: (1) increase of ambient temperature followed by a triaxial compression test, (2) triaxial compression test followed by a confined heating phase. Results show that: (1) under anisotropic mechanical boundary conditions, heating produces damage, (2) higher temperature induces larger damage and deformation, (3) degradation of rock toughness due to an increase in temperature affects the damage threshold. The proposed framework is expected to bring new insights in the design and reliability assessment of geotechnical reservoirs and repositories, such as nuclear waste disposals, geothermal systems, carbon dioxide sequestration systems, and high-pressure gas reservoirs.

1. INTRODUCTION

The Excavation Damage Zone (EDZ) has to be assessed in order to design safe and sustainable underground geotechnical facilities. In addition to mechanical damage, nuclear waste repositories and geothermal systems are also exposed to important temperature gradients over time: deep nuclear waste repositories are basically underground cavities, in which radioactive waste is disposed. Radioactive waste releases heat with an exponent decay of power, responsible for a long-term increase in the temperature of surrounding rock [1]. The dramatic changes in temperature associated with geothermal reservoir exploitation also affect rock properties [2]. This raises the necessity to formulate accurate thermo-mechanical damage models for rock.

Continuum Damage Mechanics (CDM) provides a theoretical framework to model the effects of cracking on deformation and stiffness. The approach is purely energetic and does not require a geometric description of the crack pattern. The second-order tensor defined by Kachanov [3] is particularly well-suited to evaluate damaged elastic properties of a solid with non-interacting cracks. Most of the models of thermo-mechanical damage proposed for rock are associated with a form of crack-induced volumetric cracking, which can be captured by a "dilatancy boundary", like in salt rock for instance [4, 5]. This class of models (see also [6]) do not capture stiffness changes [6] and could not predict damage-induced anisotropy in a sedimentary rock. A thermo-mechanical damage model was proposed by Zhou *et al*. [7], in which a scalar damage variable is injected in plastic and viscoplastic hardening laws, and is used to model stiffness degradation. Irreversible deformation is considered rate-dependent, but damage itself is considered rate-independent. Miao *et al*. [8] explained a more general thermodynamic framework that allows modeling anisotropic effects of damage and healing on deformation and stiffness, for both rate-dependent and rate-independent damage processes.

In general, two flow rules are needed to close the model formulation: the rate of inelastic deformation and the rate of damage (affecting the stiffness tensor). Laboratory tests [9, 10], and in-situ tests [11] have been carried out to understand the effect of thermal damage on the physical properties (e.g. microstructure, bulk density, and effective porosity) of various rocks, which could serve as a basis to postulate the form of energy potentials involved in the initiation and propagation of thermo-mechanical damage - at the scale of a Representative Elementary Volume (REV).

The goal of this research is to formulate an anisotropic thermo-mechanical damage model for rocks. The general framework of the thermo-mechanical damage model is presented in Section 2. The proposed model has been implemented in MATLAB to simulate two different loading paths: (1) increase of ambient temperature followed by a triaxial compression test, (2) triaxial compression test followed by a confined heating phase. Results are presented in Section 3.

2. OUTLINE OF THE ANISOTROPIC THERMO-MECHANICAL DAMAGE MODEL

2.1. Thermo-mechanical free energy of the damaged rock skeleton

A hyper-elastic framework is adopted [12], i.e. it is assumed that the elasticity tensor derives from an energy potential. Stress is conjugate to elastic deformation. The damage variable (noted Ω) is defined as the second-order crack density tensor [3]. Assuming that rock has a linear thermo-elastic behavior in the absence of damage, the free energy of the rock solid skeleton is sought in the form of a polynomial of order two in elastic deformation and temperature. Taking Halm & Dragon's rock mechanical damage model as a reference, it is assumed that the free energy should be a linear function of damage [13]. Rock skeleton free energy is expressed as:

$$\Psi_S(\varepsilon^E,\tau,\Omega) = \frac{1}{2}\varepsilon^E{:}\,D(\Omega){:}\,\varepsilon^E + g\Omega{:}\,\varepsilon - \frac{1}{2\tau_0}C(\Omega)\tau^2 - \tau K(\Omega){:}\,\varepsilon^E \quad (1)$$

in which the damage elastic strain energy is expressed in the same way as in Halm & Dragon's model, but in terms of elastic deformation (ε^E) instead of total deformation (ε) in order to stay in the framework of hyper-elasticity:

$$\frac{1}{2}\varepsilon^E{:}\,D(\Omega){:}\,\varepsilon^E = \frac{1}{2}\lambda(tr\varepsilon^E)^2 + \mu tr(\varepsilon^E\cdot\varepsilon^E) + \alpha tr\varepsilon^E tr(\varepsilon^E\cdot\Omega) + 2\beta tr(\varepsilon^E\cdot\varepsilon^E\cdot\Omega) \quad (2)$$

in which $D(\Omega)$ is the damaged stiffness tensor. The term $g\Omega{:}\,\varepsilon$ is kept unchanged from Halm & Dragon's formulation, and represents the energy that needs to be released to close residual cracks. The two last terms of free energy ($-\frac{1}{2\tau_0}C(\Omega)\tau^2 - \tau K(\Omega){:}\,\varepsilon^E$) are the classical linear thermo-elastic energy potentials, in which material properties have been made dependent on damage. λ and μ are Lamé coefficients, g, α, and β are damaged material parameters, τ_0 is the initial temperature, τ is the temperature change, $C(\Omega)$ is the damaged heat capacity, $K(\Omega)$ is the product of the damaged bulk modulus ($k(\Omega)$) by the solid skeleton thermal expansion coefficient (α_T). Cracks are assumed to reduce the effective material surface that can resist internal forces. However, in the undamaged part of the bulk (i.e. outside the cracks), solid properties are unchanged. That is the reason why the thermal expansion coefficient α_T is assumed to remain constant, while the bulk modulus $k(\Omega)$ depends on damage.

Conjugation relationships provide the expressions of stress and damage-driving force, with the damage-driving force further decomposed into two parts:

$$\sigma = \frac{\partial\Psi_S(\varepsilon^E,\tau,\Omega)}{\partial\varepsilon^E} = D(\Omega){:}\,\varepsilon^E + g\Omega - \tau K(\Omega) \quad (3)$$

$$Y = -\frac{\partial\Psi_S(\varepsilon^E,\tau,\Omega)}{\partial\Omega} = Y_1 + Y_2 \quad (4)$$

$$Y_1 = -g\varepsilon - \alpha(tr\varepsilon)\varepsilon - 2\beta(\varepsilon\cdot\varepsilon) \quad (5)$$

$$Y_2 = \frac{1}{2\tau_0}\frac{\partial C(\Omega)}{\partial\Omega}\tau^2 + \tau\frac{\partial K(\Omega)}{\partial\Omega}{:}\,\varepsilon^E \quad (6)$$

2.2. Incremental constitutive relationships

Stress evolution can be derived from Equation 3:

$$d\sigma = D(\Omega){:}\,d\varepsilon^E + \left(\frac{\partial D(\Omega)}{\partial\Omega}{:}\,\varepsilon^E\right){:}\,d\Omega + \mathrm{g}d\Omega - K(\Omega)d\tau - (\frac{\partial K(\Omega)}{\partial\Omega}d\Omega)\tau \quad (7)$$

The total deformation tensor is split into three components referring to [14], as shown in Figure 1:

$$\varepsilon = \varepsilon^e + \varepsilon^{ed} + \varepsilon^{id} = \varepsilon^E + \varepsilon^{id} \quad (8)$$

in which ε^e is the purely elastic deformation, which would be recovered by unloading in the absence of damage. ε^{ed} is the additional elastic deformation associated with the change of stiffness due to damage. ε^{id} is the irreversible deformation induced by damage, representing residual cracks that remain open after unloading. Total elastic deformation is the sum of purely elastic and damage-induced elastic deformation: $\varepsilon^E = \varepsilon^e + \varepsilon^{ed}$. The increment of elastic deformation is split into a mechanical and a thermal component:

$$d\varepsilon^E = d\varepsilon^{EM} + d\varepsilon^{ET} \quad (9)$$

The damage criterion is expressed as the difference between the norm of an energy release rate and an energy threshold. The latter can depend on hardening variables. Only certain components of the thermodynamic variable conjugate to damage (***Y***) are expected to contribute to crack propagation, mainly: mechanical and thermal tensile stress maintaining cracks open after unloading. In addition, rock toughness is expected to decrease with a temperature increase. The purpose of the following development is to define a function for the energy release rate involved in the damage criterion, according to physical trends explained above.

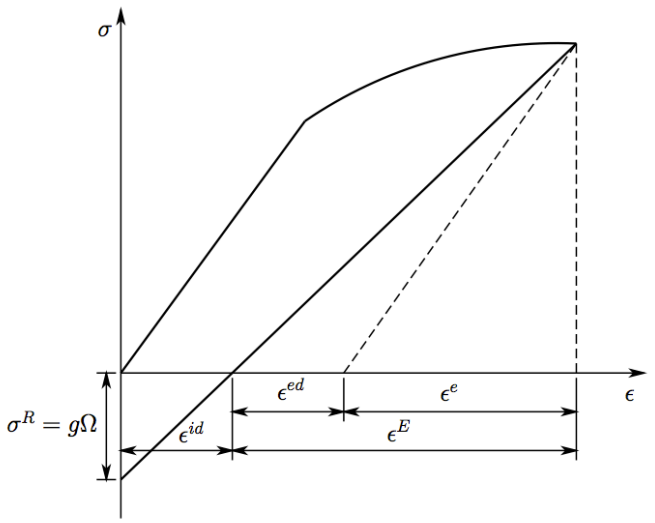

Fig. 1. Decomposition of deformation for a typical loading and unloading cycle.

The damage driving force component Y_1 (Eqn. 5) is decomposed into:

$$Y_1 = Y_{1a} + Y_{1b},$$
$$Y_{1a} = -g\varepsilon, Y_{1b} = -\alpha(tr\varepsilon)\varepsilon - 2\beta(\varepsilon \cdot \varepsilon) \quad (10)$$

$$Y_{1a}{}^{+} = -g\varepsilon^{+}, Y_{1a}{}^{-} = -g(\varepsilon - \varepsilon^{+}) \quad (11)$$

In mode I crack propagation, it is assumed that $Y_{1a}{}^{+}$ will be the dominating damage-driving force. Note that according to Equation 9, $Y_{1a}{}^{+}$ accounts for tensile deformation due to internal tensile forces induced by mechanical stress or temperature increase. Y_2 (Eqn. 6) accounts for the change of rock properties due to temperature changes ($Y_2 = 0$ in a purely mechanical damage model). A quick dimensional analysis indicates that the derivative of heat capacity relative to damage is several orders of magnitude smaller than the derivative of the bulk modulus with damage. For this reason, the term $\frac{1}{2\tau_0}\frac{\partial C(\Omega)}{\partial \Omega}\tau^2$ is neglected in the definition of the damage-driving force. Using the definition of the bulk modulus, and combining Equations 2 and 6, we can show that Y_2 should be proportional to $\alpha_T(\alpha + 2\beta)\tau$, and should vary like a polynomial of order one in elastic deformation. In addition, inter-particle distance in the rock matrix increases with temperature. At higher temperatures, it requires more energy to propagate a crack so as to increase the distance between rock particles. As a result, the force Y_2 should counter-act the tensile damage-driving force $Y_{1a}{}^{+}$. Therefore, the following thermal damage-driving force is defined:

$$Y_2{}^{d} = A \cdot \tau \cdot \alpha_T(\alpha + 2\beta)tr(\varepsilon^{E+}) \quad (12)$$

where ε^{E+} is the tensile elastic deformation, which indicates the increase of inter-particle distance under high temperature. A is a proportionality constant. As a conclusion, the total damage-driving force retained in the proposed thermo-mechanical damage model (noted $Y_d{}^{+}$) is defined as:

$$Y_d{}^{+} = Y_{1a}{}^{+} + Y_2{}^{d}$$
$$= -g\varepsilon^{+} + A \cdot \tau \cdot \alpha_T(\alpha + 2\beta)tr(\varepsilon^{E+}) \quad (13)$$

The damage criterion is written in the form of "norm of force – threshold":

$$f_d(Y_d{}^{+}, \Omega) = \sqrt{\frac{1}{2}\, Y_d{}^{+} : Y_d{}^{+}} - (C_0 + C_1\Omega) \quad (14)$$

in which C_0 is the initial damage threshold which is necessary to trigger damage, and C_1 is a parameter which controls crack growth with cumulated damage. Using the consistency conditions (i.e., $f_d = 0, \dot{f}_d = 0$), the increments of Lagrange multiplier and damage are calculated as:

$$d\lambda_d = -\frac{\frac{\partial f_d}{dY_d{}^{+}} : dY_d{}^{+}}{\frac{\partial f_d}{\partial \Omega} \cdot \frac{\partial f_d}{\partial Y_d{}^{+}}} = \frac{Y_d{}^{+} : dY_d{}^{+}}{(C_1\delta) : Y_d{}^{+}} \quad (15)$$

$$d\Omega = d\lambda_d \frac{\partial f_d(Y_d{}^{+}, \Omega)}{\partial Y_d{}^{+}}$$
$$= \frac{[\frac{Y_d{}^{+}}{\sqrt{2\, Y_d{}^{+} : Y_d{}^{+}}}] : dY_d{}^{+}}{(C_1\delta) : [\frac{Y_d{}^{+}}{\sqrt{2\, Y_d{}^{+} : Y_d{}^{+}}}]} : [\frac{Y_d{}^{+}}{\sqrt{2\, Y_d{}^{+} : Y_d{}^{+}}}] \quad (16)$$

3. SIMULATIONS

3.1. Description of the thermo-mechanical stress-paths simulated

The thermo-mechanical damage model described in section 2 has been implemented in MATLAB. Cylindrical rock samples and axis-symmetric conditions are assumed. A triaxial compression test is simulated to incorporate thermal effects. Two sequences of thermo-mechanical axis-symmetric tests are carried out (Fig.2):

- Isotropic compression → axial compression at constant temperature and constant lateral stress → increase of temperature under the constraint under the constraint of zero axial deformation.
- Isotropic compression → increase of temperature under the constraint under the constraint of zero axial deformation → axial compression at a new ambient temperature

Each loading sequence comprises three phases:

(1) Isotropic compression (M1)
An isotropic compression is applied by stress-controlled loading. The confining pressure is chosen

so as to ensure that the damage criterion is not reached: during this phase (M1), the material remains elastic.

(2) Triaxial compression (M2)

The sample is loaded by increasing the axial strain (direction 1) at a constant strain rate. The lateral stresses do not change throughout this phase (M2).

(3) Confined heating (TM)

Axial deformation is fixed while the temperature increases. Lateral expansion is allowed with lateral stresses unchanged. This phase is categorized as a thermo-mechanical phase (TM).

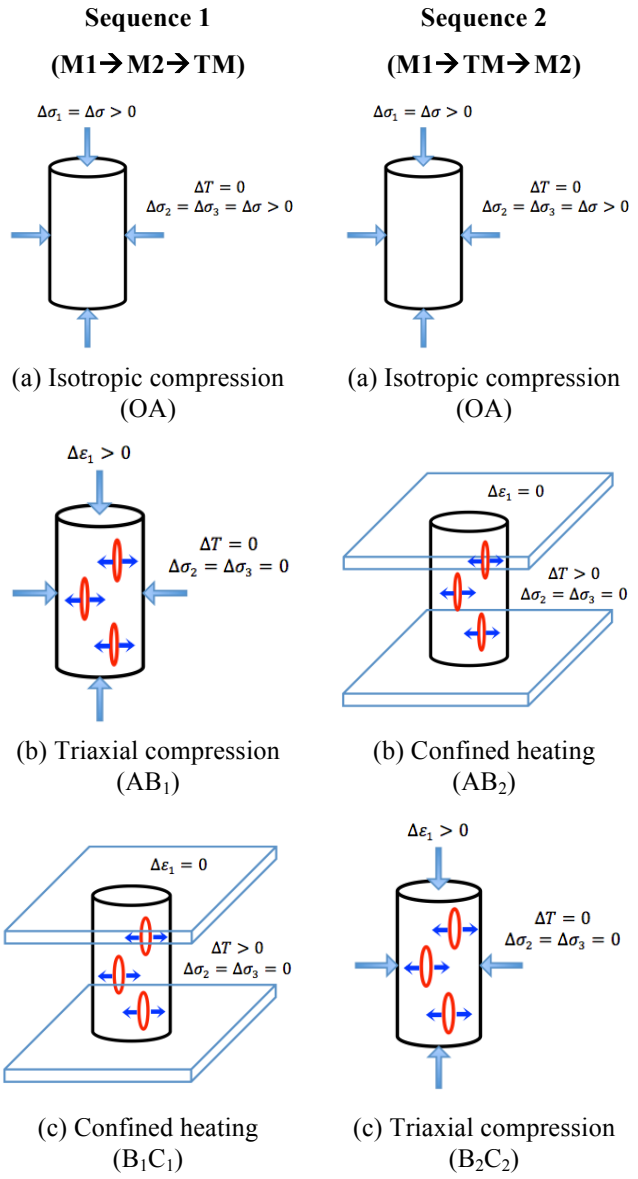

Fig. 2. Loading paths for the simulation of thermo-mechanical axis-symmetric tests

3.2. *Results: thermo-mechanical test*

Mechanical and damage parameters are taken equal to the ones calibrated by Halm and Dragon [13] for Fontainebleau sandstone. For the thermal expansion coefficient, a standard value for typical rock materials is used (Table 1).

An isotropic compression of 15 MPa is applied at the beginning. It is followed by the two sequences described in Section 3.1. During the axial compression phase at constant radial confining pressure, the maximum axial strain is 0.00526. Temperature is increased by 200K from the initial room temperature (assumed 293K).

Table 1. Material parameters used in the simulation

$\lambda\ (Pa)$	$\mu\ (Pa)$	$\alpha\ (Pa)$	$\beta\ (Pa)$
2.63×10^{10}	1.75×10^{10}	1.9×10^{9}	-2.4×10^{10}
$g\ (Pa)$	$C_0\ (Pa)$	$C_1\ (Pa)$	$\alpha_T\ (K^{-1})$
1.1×10^{8}	1000	5.5×10^{5}	-1×10^{-5}

During the triaxial compression phase (M2), deviatoric stress generates lateral tensile strain, causing lateral damage (Ω_1=0, Ω_2=Ω_3≠0). In both sequences, a degradation of rock stiffness can be observed during phase (M2) (Fig.3). In both sequences, deviatoric stress q increases when the temperature increases (OB_2 & B_1C_1). This is due to the mechanical boundary conditions: axial thermal expansion in constrained, which generates compressive internal stress – in virtue of the action/reaction principle. Temperature-induced compression adds to mechanical compression. Damage induced during phase AB_1 (mechanical axial compression) lowers stiffness, which explains why during the heating phase (B_1C_1), the thermal compressive stress developed in reaction to thermal expansion is smaller than OB_2. In the stress/strain diagrams in Fig.3 (for lateral strain in particular), slope OB_2 of sequence 2 is smaller than slope AB_1 of sequence 1, i.e. purely mechanical compression generates damage "more effectively" than thermo-mechanical force.

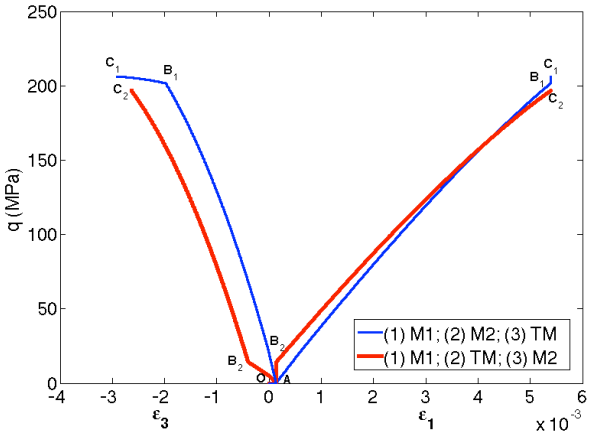

Fig. 3. Deviatoric stress versus axial and lateral deformation: thin line – sequence 1; thick line – sequence 2.

After the whole loading programs of three phases, sequence 2 gives less damage than sequence 1 (Fig. 4a & 4b, Fig.5). This could be expected from the model formulation: in sequence 2, we apply a mechanical loading in a heated material, in which the "counter-acting" damage driving force Y_2^d defined in Equation 12 is larger – meaning that overall the damage driving force Y_d^+ defined in Equation 13 is smaller, and therefore, the energy released to open cracks is less. Moreover, the comparison of the rate of damage in Fig.4a indicates that lateral damage progresses faster in a cooler sample (slope $A'B_1$ > slope B_2C_2; segment AA' represents the purely elastic range).

In both sequences, the sample expands laterally (due to mechanical or thermo-mechanical compression). As could be expected, larger damage results in larger deformation, and lateral strains obtained at the end of sequence 1 are larger than at the end of sequence 2 (Fig. 4b). In sequence 1, damage induced by mechanical compression increases the required energy release rate (Eqn. 14), in order to further propagate cracks in the heating phase (slope of B_1C_1 < slope of $A'B_1$ in Fig.4b). On the other hand, for sequence 2, thermo-mechanical stress induced damage and higher ambient temperature both contribute to the increase of the damage threshold; as a result, slope of B_2C_2 is smaller than $A'B_2$ (Fig.4b).

In summary, the ordered sequence of the slopes is $A'B_1 > A'B_2 > B_2C_2 > B_1C_1$.

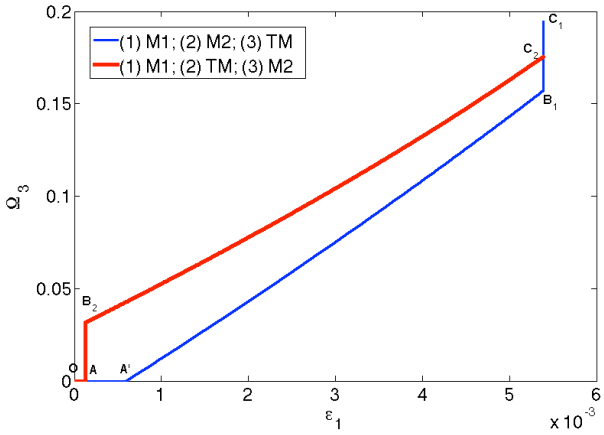

(a)

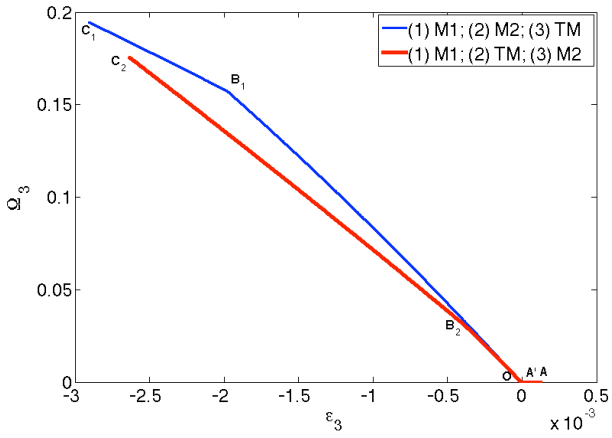

(b)

Fig. 4. Damage evolution with respect to deformation: (a) radial damage component versus axial deformation, (b) radial damage component versus lateral deformation. (thin line – sequence 1; thick line – sequence 2)

In sequence 2, there is a threshold temperature change (about 62 K) for thermo-mechanical stress induced damage to occur. On the contrary, damage starts to develop immediately after the temperature increase in sequence 1 (Fig.5).

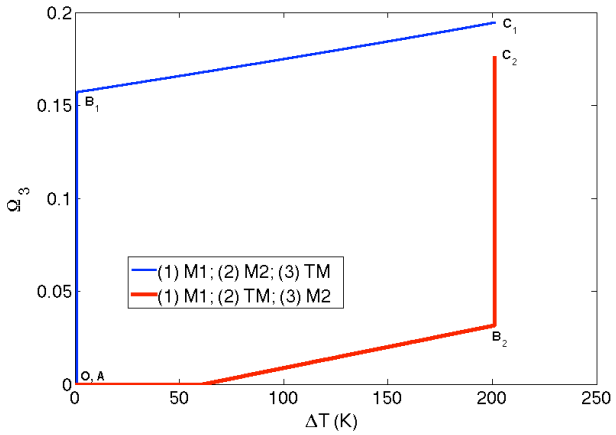

Fig. 5. Damage evolution with respect to temperature variation

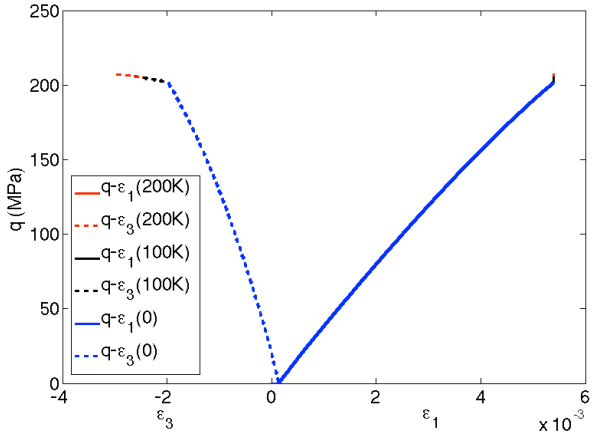

Fig. 6. Deviatoric stress versus axial and lateral deformation (sequence 1)

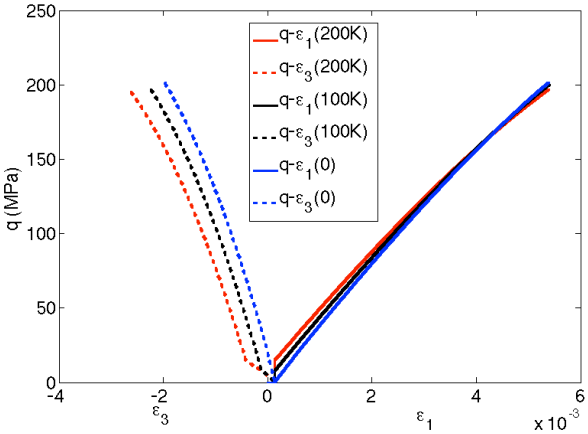

Fig. 9. Deviatoric stress versus axial and lateral deformation (sequence 2)

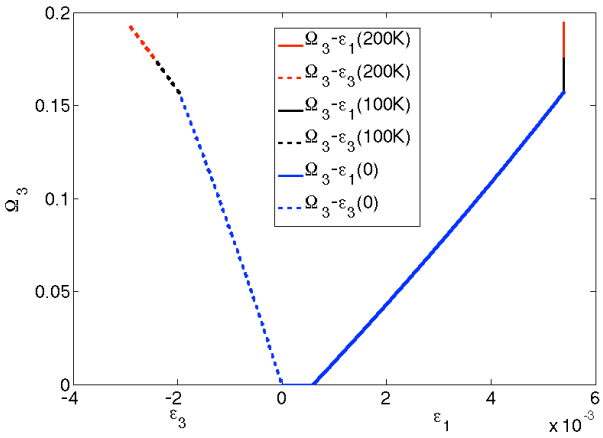

Fig. 7. Damage evolution with respect to axial and lateral deformation (sequence 1)

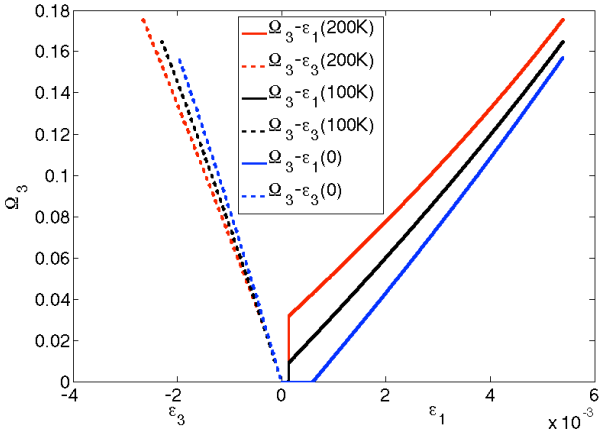

Fig. 10. Damage evolution with respect to axial and lateral deformation (sequence 2)

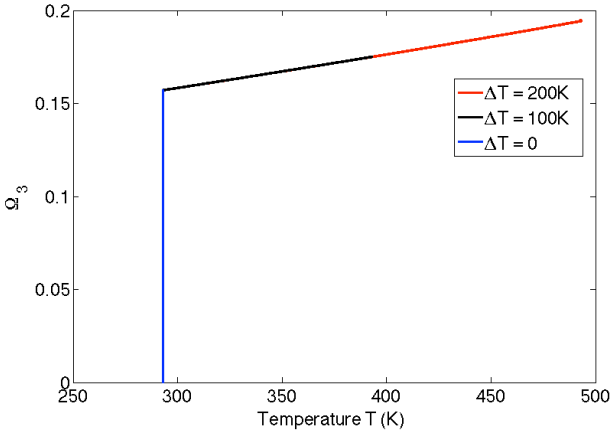

Fig. 8. Damage evolution with respect to temperature (sequence 1)

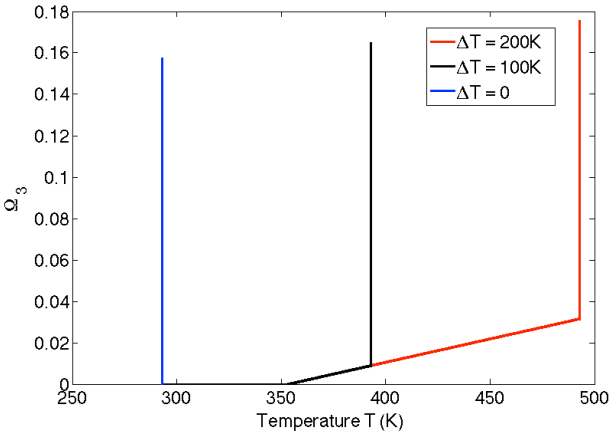

Fig. 11. Damage evolution with respect to temperature (sequence 2)

3.3. Effect of ambient temperature on triaxial compression tests

A parametric study is conducted to investigate the influence of ambient temperature on the results obtained during the axis-symmetric thermo-mechanical test. The maximum axial strain in phase M2 is still taken as 0.00526. For both sequences, three ambient temperature values are adopted, 293K, 393K, and 493K (i.e. the temperature increments are 0, 100K, and 200K, respectively).

(1) Sequence 1

As described in Fig.2, the purely mechanical compression test is simulated first followed by an increase of temperature (three different levels of temperature are simulated). The stress-strain diagram reveals that higher temperature generates larger deviatoric stresses and lateral expansion (Fig. 6).

Expansion of the sample along the lateral direction indicates the generation of more lateral damage (Fig. 7). Lateral damage induced by thermo-mechanical effect also increases with ambient temperature (Fig. 8).

(2) Sequence 2

The ambient temperature of the sample under confinement is raised to certain levels first, before the purely mechanical compression is applied. Because of the variation in ambient temperature, rock samples exhibit different stress-strain behaviors (Fig. 9). Slopes of the curves representing material stiffness drop with increasing temperature (meaning that more damage has been produced). Similar to sequence 1, larger lateral expansion is also observed under higher ambient temperature.

At higher temperatures, it requires more energy to increase the distance between rock particles by propagating a crack. In addition, because of the cumulated damage in the heating phase, it requires larger damage-driving force to create new damage (refer to Eqn. 14). So the damage-changing rate (slope of damage/strain diagram) decreases when temperature rises (Fig.10). Damage does not increase at the beginning of the heating phase (Fig.11). This further validates the existence of the threshold temperature at about 355K (=293K+62K) for the simulated rock sample.

4. CONCLUSION

A thermodynamic framework is proposed to model anisotropic thermo-mechanical damage in rock. The model is based on Continuum Damage Mechanics, with damage defined as the second-order crack density tensor [3]. Halm and Dragon's model [13] is used as a basis to postulate the form of the free energy, which is expressed in the form of a polynomial of deformation, temperature and damage. Thermo-elastic energy potentials are made dependent on damage - by assuming that in addition to the bulk modulus, heat capacity is affected by damage. Stress and the damage-driving force are derived from the free energy, and conjugation relationships indicate that stress and damage driving force depend on internal variables (such as damage) and external variables (e.g., strain and temperature). The energy release rate controlling damage propagation is a modified damage driving force. The damage criterion controls mode I crack propagation, captures temperature-induced decrease of rock toughness, and accounts for the increase of energy release rate necessary to propagate cracks in a damaged medium.

Two thermo-mechanical loading paths have been simulated with MATLAB: (1) isotropic confining phase followed by axial compression, followed by heating phase; (2) isotropic confining phase followed by a heating phase, followed by an axial compression. Results show that under anisotropic mechanical boundary conditions, cracks can be produced during heating. Higher ambient temperature increases the lateral expansion and produces more damage. In the proposed model formulation, the thermo-mechanical energy release rate increases with thermal dilation, but decreases with ambient temperature. In general, the evolution of the damage-driving force reflects the increase of the damage threshold as temperature is raised. This explains why lateral damage progresses faster in a cooler sample. It is also found that in the lab tests simulated, there is a temperature threshold, below which intact rock behaves elastically.

Further work will be dedicated to model validation and calibration against published experimental data, and to the modeling of the coupled effects of crack opening, closure (unilateral effects on stiffness) and healing ("bilateral" mechanical recovery).

REFERENCES

1. Liang, W.G., S.G. Xu, and Y.S. Zhao. 2006. Experimental study of temperature effects on physical and mechanical characteristics of salt rock. *Rock Mech Rock Eng.* 39(5): 469-482.
2. McDermott CI, ARL Randriamanjatosoa, H. Tenzer, and O. Kolditz. 2006. Simulation of heat extraction from crystalline rocks: the influence of coupled processes on differential reservoir cooling. *Geothermics*. 35: 321-344.
3. Kachanov, M. 1992. Effective elastic properties of cracked solids: critical review of some basic concepts. *Appl. Mech. Rev. (ASME)*. 45(8): 304-335.

4. Hunsche, U. and A. Hampel. 1999. Rock salt – the mechanical properties of the host rock material for a radioactive waste repository. *Engineering Geology*. 52(3): 271-291.

5. Hou, Z. 2003. Mechanical and hydraulic behavior of rock salt in the excavation disturbed zone around underground facilities. *International Journal of Rock Mechanics and Mining Sciences*. 40(5): 725-738.

6. Chan, K.S., S.R. Bodner, and D.E. Munson. 2001. Permeability of WIPP salt during damage evolution and healing. *International Journal of Damage Mechanics*. 10(4): 347-375.

7. Zhou, H., D. Hu, F. Zhang, and J. Shao. 2011. A thermo-plastic/viscoplastic damage model for geomaterials. *Acta Mech Solida Sinica*. 24(3): 195-208.

8. Miao, S., M. Wang, and H. Schreyer. 1995. Constitutive models for healing of materials with application to compaction of crushed rock salt. *J. Eng. Mech*. 121(10): 1122-1129.

9. Yavuz, H., S. Demirdag, S. Caran. 2009. Thermal effect on the physical properties of carbonate rocks. *International Journal of Rock Mechanics and Mining Sciences*. 47(1): 94-103.

10. Chaki, S., M. Takarli, and W.P. Agbodjan. 2008. Influence of thermal damage on physical properties of a granite rock: Porosity, permeability and ultrasonic wave evolutions. *Construction and Building Materials*. 22(7): 1456-1461.

11. Lan, H. and C.D. Martin, and J.C. Andersson. 2013. Evolution of in situ rock mass damage induced by mechanical-thermal loading. *Rock Mech Rock Eng*. 46(1): 153-168.

12. Houlsby, G.T. and A.M. Puzrin. 2006. *Principles of hyperplasticity, an approach to plasticity theory based on thermodynamic principles.* London: Springer-Verlag.

13. Halm, D. and A. Dragon. 1998. An anisotropic model of damage and frictional sliding for brittle materials. *Eur. J. Mech. A/Solids*. 17(3): 439-460.

14. Abu Al-Rub, R.K. and G.Z. Voyiadjis. 2003. On the coupling of anisotropic damage and plasticity models for ductile materials. *International Journal for Solids and Structures*. 40(11): 2611-2643.